

REDSHIFT CLUSTERING IN THE HUBBLE DEEP FIELD¹

JUDITH G. COHEN², LENNOX L. COWIE³, DAVID W. HOGG⁴, ANTOINETTE SONGAILA³, ROGER BLANDFORD⁴, ESTHER M. HU³ AND PATRICK SHOPBELL²

ABSTRACT

We present initial results from a redshift survey carried out with the Low Resolution Imaging Spectrograph on the 10 m W. M. Keck Telescope in the Hubble Deep Field. In the redshift distribution of the 140 extragalactic objects in this sample we find 6 strong peaks, with velocity dispersions of $\sim 400 \text{ km s}^{-1}$. The areal density of objects within a particular peak, while it may be non-uniform, does not show evidence for strong central concentration. These peaks have characteristics (velocity dispersions, density enhancements, spacing, and spatial extent) similar to those seen in a comparable redshift survey in a different high galactic latitude field (Cohen et al 1996), confirming that the structures are generic. They are probably the high redshift counterparts of huge galaxy structures (“walls”) observed locally.

Subject headings: Cosmology: observations — Galaxies: redshift and distances — Large-scale structure of Universe

1. INTRODUCTION

The Hubble Deep Field (HDF hereafter; Williams et al 1996) has been surveyed to extraordinary depths, with point source detection limits around 29 mag in the V and I bands, in an intensive campaign by the Hubble Space Telescope in 1995 December. The images represent the deepest images ever taken in the optical and have already provided the basis for studies of deep visual counts (Williams et al 1996), faint object morphology

¹Based in large part on observations obtained at the W.M. Keck Observatory, which is operated jointly by the California Institute of Technology and the University of California

²Palomar Observatory, Mail Stop 105-24, California Institute of Technology

³Institute for Astronomy, University of Hawaii, 2680 Woodlawn Drive, Honolulu, Hawaii 96822

⁴Theoretical Astrophysics, California Institute of Technology, Mail Stop 130-33, Pasadena, CA 91125

(Abraham et al 1996), gravitational lensing (Hogg et al 1996), and high-redshift objects (Steidel et al 1996; Clements & Couch 1996). These studies represent only the beginning of a large number of scientific projects possible with the HDF data.

In this paper we present the first results of a ground based spectroscopic survey of galaxies in the HDF with the Keck Telescope. These observations were taken in order to provide a database of object redshifts for the use of the astronomical community and in order to expand the faint object redshift surveys of Cowie et al (1996) and Cohen et al (1996) to an additional field.

We assume an Einstein - de Sitter universe ($q_0 = 0.5$) with a Hubble constant $100h$ km s⁻¹Mpc⁻¹.

2. REDSHIFT SAMPLE

The HDF was selected on the basis of high galactic latitude, low extinction, and various positional constraints described by Williams et al (1996). Redshifts were acquired with the Low Resolution Imaging Spectrograph (Oke et al 1995) on the 10 m W. M. Keck Telescope over two rectangular strips 2 x 7.3 arcmin² centered on the HST field in 1996 January, March and April. One strip was aligned east-west while the second was aligned at a position angle of 30° to maximize the slit length that fell within the HDF itself, where the two strips overlap.

The sample selection is different in each of the two strips. The photometry and the definition of the sample for spectroscopic work are described in Paper II of this series, Cowie et al (1997). Plans exist to complete the sample in a number of photometric bandpasses, but in view of the great interest in the HDF and the many follow up studies in progress, we present this data before the complete sample is available.

Table 1 presents the redshifts of 140 extragalactic objects, about half of which are in the HDF itself and the remainder in the flanking fields. The median redshift z of the extragalactic objects in the present sample is $z = 0.53$. Only three are quasars or broad-lined AGNs. 12 Galactic stars were found as well. The radial velocity precision of our redshifts is unusually high for a deep redshift survey. We estimate that the uncertainty in z for those objects with redshifts considered secure and accurate is ≈ 300 km s⁻¹. Coordinates, crude ground based R magnitudes in a 3 arc-sec diameter intended for object identification only, and redshifts are given in Table 1.

A more detailed account of the photometric and spectroscopic properties of the entire

sample including photometry from U through K as well as a discussion of incompleteness in the sample selection and redshift identification is in preparation. These incompletenesses ought not to affect the present work.

3. REDSHIFT DISTRIBUTION

3.1. Velocity Peaks

The redshift histogram over the region $0.2 < z < 0.9$ is shown in Figure 1. It shows clear evidence of clustering. Velocity peaks were identified by choosing bins of variable width and centers so as to maximize their significance relative to occurring by chance in a smoothed velocity distribution (smoothing width $20,000 \text{ km s}^{-1}$) derived from the present sample (c.f. Cohen et al 1996). Using this procedure we isolate 6 peaks significant at better than 99.5 percent confidence (see Table 2). The fourth column in Table 2 gives a statistical significance parameter X_{max} . The fifth and sixth columns give the comoving transverse size corresponding to 1 arc-min and the comoving radial distance corresponding to $\Delta z = 0.001$. The density in velocity space within these peaks exceed the average density by a factor that ranges from 4 to as high as 30 for the peak at $z_p = 0.321$. 40 percent of the total sample lies within these peaks. Larger peaks including outliers are also highly significant. The local velocity dispersions for these peaks are strikingly small, ranging from 170 km s^{-1} to 600 km s^{-1} . These are upper bounds because they are comparable with our measurement errors. They are also similar to the results obtained in a high latitude field for which we carried out a deep redshift survey with LRIS earlier (Cohen et al 1996).

By itself, this sample is too small to measure the two point correlation function in velocity space. However, there is a 5σ excess correlation in the $500\text{--}1000 \text{ km s}^{-1}$ interval with a correlation scale $V_0 \sim 600 \pm 200 \text{ km s}^{-1}$ (c.f. Carlberg et al. (1997), Le Fèvre et al. 1996) which can be converted into comoving distance along the line of sight using the data in the sixth column of Table 2. There is no evidence for correlation with velocity differences in excess of 1000 km s^{-1} . No distinction between low and high redshift is discernible. There is no evidence for periodicity in the peak redshifts (c.f. Broadhurst et al 1990).

3.2. Morphology Correlation

If we make a simple morphological separation of the galaxies in the redshift survey into spirals, ellipticals and Peculiar/Mergers and use the HST images of the HDF and of the

flanking fields to classify these galaxies (c.f. van den Bergh et al 1996), we find there is no indication of any difference in population between the background field galaxies and those in the redshift peaks. In particular, the redshift peaks do not contain a detectable excess of elliptical galaxies.

4. ANGULAR DISTRIBUTION

The angular distribution of the entire sample and of the galaxies in the two most populous velocity peaks is shown in Figure 2. The peculiar shape is caused by the use of two LRIS strips with different position angles. The outline of the area covered is indicated by the solid lines, while the outline of the area of the WFCII observations in the HDF is indicated by the dashed lines. The galaxies associated with the 6 velocity peaks mostly exhibit a non-uniform distribution, though none show the strong central concentration characteristic of clusters. The redshift sample must be completed before it is possible to make quantitative statements.

4.1. Areal Density

The areal density of galaxies brighter than $0.1L^*$ (as defined at K) is computed for redshift peaks in the 0 hour field (Cohen et al 1996) and for the two largest peaks in the HDF, where the K photometry is not fully assembled yet. Corrections have been applied for galaxies below the magnitude cutoff of the survey assuming a flat luminosity function at the faint end. To investigate a local analog to these structures, this is repeated for the Local Group, for the Virgo cluster (within a radius of 6° degrees from its center) using the survey of Kraan-Korteweg (1981) and within the core of the Coma Cluster using data from Thompson & Gregory (1980). In these local structures, the luminosity is determined at B rather than at K . The results are given in Table 3, and suggest that the best local analog is the region of the Virgo cluster within 6° of its center, but although the areal density is a reasonable match, the velocity dispersion in the high redshift peaks is lower, often significantly lower, than one sees in the central region of the Virgo cluster.

5. DISCUSSION

5.1. Effects of sample definition decisions

The conclusion of Cohen et al (1996), i.e., that a large fraction of the galaxy population at redshifts to unity lie in low velocity-dispersion structures, was based on a single field, but the confirmation of strong redshift-space clustering in the HDF suggests that the results are generic. The clustering seen here is stronger than that seen in other local and high-redshift surveys (Landy et al 1996, LeFèvre 1996, etc.) The difference is attributed most importantly to the high sampling density in a small field.

5.2. Structure Morphology

At one level, these peaks may be no more than a manifestation of the fact that galaxies are correlated in both configuration and velocity space. The connection between spatial and velocity correlation functions is quite model-dependent (e.g. Brainerd et al. 1996). Conversely, if we can gain an empirical understanding of this relationship, it can discriminate among cosmogonic models. We briefly comment upon some possibilities.

One explanation is that the velocity peaks represent structures in velocity space and are not prominent in real space. Such effects are sometimes seen in numerical simulations, e.g. Park & Gott 1991, Bagla & Padmanabhan 1994. For example, they might be a “backside infall” into a large structure where the Hubble expansion opposes the infall so as to give more or less uniform recession velocity over a large interval of radial distance. The generic kinematic difficulty with this explanation is that in order for features like this not to have many more descendants in which the velocities have long ago crossed, the characteristic lifetimes must be a significant fraction of the age of the universe which, in turn, limits the mass density contrast to small values. Given that half of the galaxies lie in these structures, a large bias parameter must be invoked.

Alternatively, we may be observing structures that are spatially compact and have the shapes of spheres, filaments, or walls. We can argue against these features being clusters on the following grounds: (i) They do not exhibit central concentrations (c.f. Sec. 4). (ii) The velocity dispersions are too small, $200 - 600 \text{ km s}^{-1}$ as opposed to $600 - 1200 \text{ km s}^{-1}$. (iii) The space density of rich clusters is too low; the Palomar Deep Cluster Survey (Postman et al 1996) finds only 7 clusters per square degree out to $z \sim 0.6$ with richness class ≥ 1 . (iv) The redshift peaks do not show the excess of ellipticals characteristic of rich clusters (Dressler 1980).

Small quasi-spherical groups are a possibility. The mean free path is $\sim 100h^{-1}$ comoving Mpc. The observed structures extend laterally over at least ~ 6 arc-min or $\sim 2h^{-1}$ Mpc,

implying a space density $\sim 3 \times 10^{-3} h^3 \text{ Mpc}^{-3}$, $\sim 1/3$ the density of L^* galaxies. Alternatively, we can associate the tentative velocity correlation scale of $V_0 \sim 600 \text{ km s}^{-1}$ with a radial extent of $\sim 4h^{-1} \text{ Mpc}$ and a lateral angular scale of ~ 12 arc-minutes at $z \sim 0.5$.

Filaments and walls have both been described in the theoretical literature (e.g. Bond et al 1996, Shandarin et al 1995). Walls dominate if there is excess power on large scales and are observed locally (e.g. in the Local Supercluster, deVaucouleurs 1975, and in local redshift surveys, de Lapparant et al 1986, Landy et al 1996). On this basis we speculate that the structures we are observing are actually walls.

There are two obvious follow up investigations which can address this hypothesis. The first is to perform similar redshift surveys in neighboring deep fields. If we assume that the wall normal is inclined at an angle θ to the line of sight and that the constituent galaxies move with the Hubble flow in two dimensions, then the variation of mean redshift with angular separation of the second survey $\Delta\phi$ and polar angle on the sky ψ is

$$\Delta z = 2[(1+z)^{3/2} - (1+z)]\Delta\phi \tan\theta \sin\psi$$

For $z = 0.5$, this is $\Delta z \sim 2 \times 10^{-4}$ per arcminute and in order to see redshift displacements in excess of the velocity dispersion, the additional surveys must be displaced by $\sim 20'$. With several lines of sight, it might be possible to test the above relation.

Secondly, wide field, multiband photometric surveys to the depth of the redshift survey are clearly important to see if there are indeed morphological and luminosity function differences between the galaxies within and outside the velocity peaks. Both investigations are underway.

We thank the Hubble Deep Field team, led by Bob Williams, for planning, taking, reducing, and making public the HDF images. We are grateful to George Djorgovski, Keith Matthews, Gerry Neugebauer, Paddy Padmanabhan, Mike Pahre, Tom Soifer and Jim Westphal for helpful conversations. The entire Keck user community owes a huge debt to Bev Oke, Jerry Nelson, Gerry Smith, and many other people who have worked to make the Keck Telescope a reality. We are grateful to the W. M. Keck Foundation, and particularly its president, Howard Keck, for the vision to fund the construction of the W. M. Keck Observatory. Support by NASA and the NSF is greatly appreciated.

Table 1. Redshifts in the Hubble Deep Field

RA (-12 ^h) m s	Dec (-62°) ' "	R_{ap} (3'') mag	z	RA (-12 ^h) m s	Dec (-62°) ' "	R_{ap} (3'') mag	z	RA (-12 ^h) m s	Dec (-62°) ' "	R_{ap} (3'') mag	z
36 21.4	12 27.1	—	0.398	36 22.0	12 37.7	21.7	0.630	36 22.2	12 41.9	20.8	0.498
36 22.7	13 00.2	20.0	0.472	36 22.9	13 46.9	20.4	0.485	36 24.9	13 01.0	20.3	0.518
36 26.5	12 52.6	20.6	0.557	36 27.7	12 41.3	20.8	0.518	36 28.1	12 38.0	21.1	0.5185
36 29.8	14 03.8	21.4	0.793	36 29.9	12 25.0	22.6	0.410	36 30.2	12 08.8	20.6	0.456
36 31.0	12 36.9	21.3	0.456	36 31.7	12 41.1	21.3	0.528	36 32.6	12 44.1	21.3	0.562
36 33.4	13 20.3	21.1	0.843	36 33.04	11 35.0	19.4	0.080	36 33.6	11 56.8	21.8	0.458
36 34.4	12 41.5	22.3	1.219	36 34.8	12 24.5	19.5	0.562	36 36.1	13 20.3	22.1	0.680
36 36.3	13 41.2	21.4	0.556	36 36.78	11 36.1	19.4	0.078	36 37.2	12 53.1	20.8	0.485
36 37.4	12 41.0	20.5	0.458	36 37.6	11 49.5	22.1	0.838	36 38.89	12 20.7	22.9	0.609
36 39.8	12 07.5	21.8	1.015	36 40.80	12 04.4	23.7	1.010	36 41.56	11 33.1	20.5	0.089
36 41.85	12 06.3	21.9	0.432	36 42.85	12 17.6	21.3	0.454	36 43.07	12 43.2	23.0	0.847
36 43.55	12 19.4	23.4	0.752	36 43.69	13 57.7	21.6	0.201	36 43.71	11 44.0	22.3	0.765
36 43.88	12 51.2	21.8	0.557	36 44.09	12 48.9	22.0	0.555	36 44.11	12 41.3	24.2	0.873
36 44.28	11 34.3	23.2	1.013	36 44.59	12 28.8	24.2	2.268	36 45.32	12 14.5	21.4	0
36 45.86	12 02.4	24.6	0.679	36 46.10	11 42.9	22.6	1.016	36 46.25	14 05.6	22.6	0.960
36 46.44	11 52.3	22.9	0.5035	36 46.45	14 08.6	23.1	0.130	36 46.68	12 38.1	23.0	0.320
36 46.78	11 45.9	23.1	1.059	36 47.21	12 31.8	23.4	0.421	36 47.99	13 10.1	21.5	0.475
36 48.5	13 29.2	23.9	0.958	36 48.51	11 42.3	23.2	0.962	36 49.29	13 12.3	22.7	0.478
36 49.34	13 47.9	19.0	0.089	36 49.42	14 07.8	22.8	0.752	36 49.55	12 58.8	22.6	0.475
36 49.64	13 14.2	22.4	0.475	36 50.15	12 40.8	21.4	0.474	36 50.18	12 46.9	22.8	0.680
36 50.63	10 59.9	21.9	0.474	36 50.73	12 56.9	23.1	0.320	36 51.0	13 21.6	20.8	0.199
36 51.02	10 32.2	21.2	0.410	36 51.35	13 01.6	22.2	0.089	36 51.61	12 21.3	22.3	0.299
36 51.69	13 54.8	22.0	0.557	36 52.03	14 58.3	22.4	0.358	36 52.39	10 36.9	22.2	0.321
36 52.59	12 21.0	24.0	0.401	36 52.68	13 55.7	22.7	1.355	36 52.71	14 32.9	21.2	0
36 52.83	14 54.7	22.7	0.463	36 52.85	14 45.1	20.1	0.322	36 53.33	12 35.2	23.4	0.560
36 53.54	15 26.0	18.7	0	36 53.57	13 09.4	22.1	0	36 53.77	12 55.0	22.0	0.642
36 54.28	14 35.1	22.8	0.577	36 54.65	13 29.1	20.0	0	36 55.44	13 54.5	22.4	1.148
36 55.45	12 46.4	23.1	0.790	36 55.50	14 00.9	23.9	0.559	36 56.26	12 42.4	19.9	0
36 56.33	12 10.4	23.7	0.321	36 56.56	12 46.8	21.7	0.5185	36 57.14	12 27.1	23.4	0.561
36 57.22	13 00.8	22.3	0.474	36 57.64	13 16.5	23.8	0.952	36 57.98	13 01.6	23.0	0.320
36 58.22	12 15.2	22.9	1.020	36 58.29	15 49.4	21.7	0.457	36 58.56	12 23.0	24.2	0.682
36 58.64	14 39.1	23.3	0.512	36 58.66	12 53.2	22.2	0.321	36 58.74	14 35.6	21.9	0.678
36 58.76	16 38.9	20.0	0.299	36 59.43	12 22.7	24.5	0.472	36 59.79	14 50.6	22.5	0.761
37 00.41	14 06.7	21.5	0.423	37 00.47	12 35.9	24.5	0.562	37 01.8	13 23.8	20.7	0.408
37 01.81	15 10.9	22.9	0.938	37 02.3	13 43.0	21.3	0.559	37 02.5	13 48.3	22.7	0.513
37 02.5	14 02.7	22.1	1.243	37 02.70	15 44.8	20.8	0.514	37 02.81	14 24.4	21.5	0.512
37 03.21	16 46.9	23.0	0.744	37 03.6	13 54.3	21.7	0.745	37 03.82	14 42.0	22.3	0.475
37 03.91	15 23.8	22.6	0.377	37 04.17	16 25.3	22.8	0.474	37 04.52	16 52.2	21.1	0.377
37 04.56	14 30.0	22.0	0.561	37 04.73	14 55.8	21.2	0	37 04.91	15 47.4	23.4	0.533
37 05.0	12 11.2	22.5	0.386	37 05.66	15 25.7	22.7	0.503	37 06.0	13 33.9	21.6	0.753
37 06.81	14 30.3	21.2	0	37 07.0	12 14.7	21.4	0.655	37 07.0	11 58.5	22.4	0.593
37 07.73	16 06.1	22.8	0.936	37 08.01	16 31.7	22.7	0	37 08.04	16 59.6	21.5	0.458
37 08.1	12 53.2	21.9	0.838	37 08.1	13 21.6	22.7	0.785	37 08.20	14 54.8	22.8	0.565
37 08.25	15 15.3	22.5	0.839	37 08.53	15 02.2	22.7	0.570	37 08.60	16 12.4	21.3	0
37 08.8	12 02.8	22.6	0.855	37 09.46	14 24.3	22.0	0.476	37 09.79	15 25.0	20.0	0.597
37 10.1	13 20.5	21.7	0.320	37 11.85	16 59.7	23.5	1.142	37 12.4	13 58.2	22.6	0.848
37 12.58	15 43.4	22.3	0.533	37 13.0	13 57.2	22.0	1.016	37 13.59	15 12.0	22.1	0.524
37 14.8	13 35.4	22.5	0.897	37 16.1	13 54.2	21.5	0.476	37 16.32	16 30.4	23.4	0
37 16.4	13 11.2	21.9	0.898	37 17.0	13 57.4	20.7	0.336	37 16.52	16 44.7	22.7	0.557
37 18.28	15 54.1	21.6	0.476	37 18.3	13 48.6	22.1	0.480	37 18.4	13 22.5	20.6	0.4755
37 18.60	16 05.0	22.5	0.558	37 22.25	16 13.1	22.6	0				

Table 2. Redshift Peaks in the Hubble Deep Field

z_p	N^a	$\sigma_v(N)^b$ (km s ⁻¹)	X_{max}^c	d_{\perp} ($\Delta(\theta)=1'$) (h^{-1} Mpc) ^d	d_{\parallel} ($\Delta(z)=0.001$) (h^{-1} Mpc) ^d
0.321	8	170	22	0.22	2.0
0.457	7	310	10	0.31	1.7
0.475	15	315	21	0.31	1.6
0.516	8	595	8	0.33	1.6
0.559	14	420	21	0.34	1.5
0.680	5	265	8	0.40	1.4

^aNumber of galaxies within the peak as determined by statistical tests.

^bNo correction for instrumental or measurement errors has been applied.

^cStatistical parameter for estimating the significance of each peak, see Cohen et al 1996.

^dComoving distances.

Table 3. Areal Density of Peaks in The Caltech 0 hour Field and in Local Structures

z_p	N_{obs} ($L > 0.1L^*$)	Comoving Area ($h^{-2} \text{ Mpc}^2$)	$n_{\text{corr}}(L > 0.1L^*)^{\text{g}}$ ($h^2 \text{ Mpc}^{-2}$)	$\sigma_v(N-1)$ (km s^{-1})
0.392	3	1.03	3	465
0.429	14	1.19	13	615
0.581	23	1.86	19	410
0.675	8	2.30	7	405
0.766	7	2.72	7	670
0.475 (HDF) ^f	7	0.51	18	315
0.559 (HDF) ^f	7	0.64	17	420
Local Structures				
Local Group	4	1.3	3 ^a	< 100
Virgo ^b	122	8.5	14 ^a	670 ^d
Coma ^c	248	2.0	125	1080 ^e

^aIndependent of h .

^bGalaxies within a 6° radius of the cluster center.

^cGalaxies within the central region 1.2° on a side

^dBinggelli, Sandage & Tammann (1985)

^eColless & Dunn (1996) (square region 2.6° on a side)

^fThe area is that of the 3 WF CCDs.

^gComoving areal density corrected for incompleteness at the faint end.

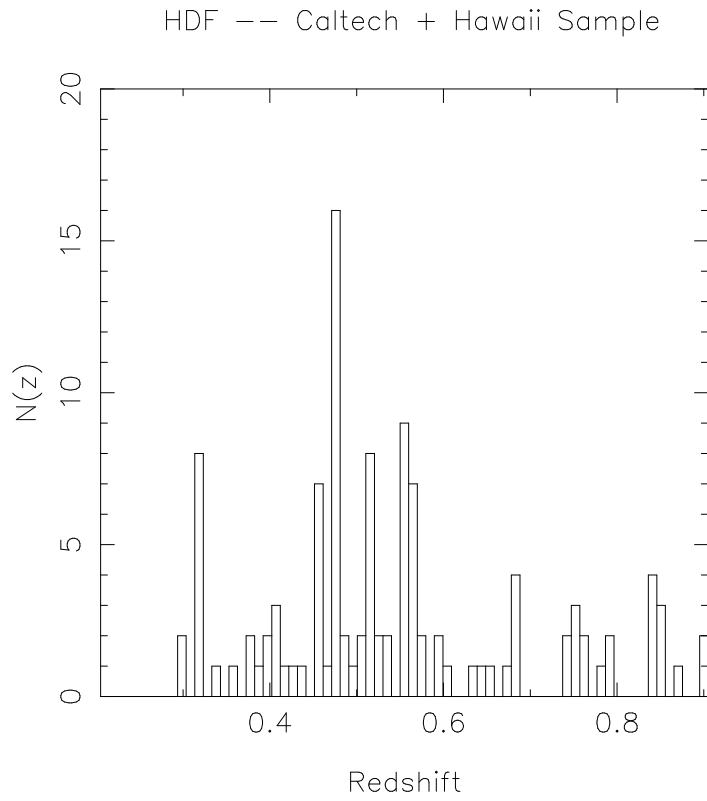
REFERENCES

- Abraham, R.G., Tanvir, N.R., Santiago, B.X., Ellis, R.S., Glazebrook, K. & van den Bergh, S., 1996, MNRAS, 279, L47
- Bagla, J.S. & Padmanabhan, T., 1994, MNRAS, 266, 227
- Bellanger, C. & de Lapparent, V., 1995, ApJ, 455, L103
- Binggelli, B., Sandage, A. & Tammann, G.A., 1985, AJ, 90, 1681
- Bond, J.R., Kofman, L. & Pogosyan, D., 1996, Nature, 380, 603
- Brainerd, T.G., Bromley, B.C., Warren, M.S. & Zurek, W.H., 1996, ApJL, 464, L103
- Broadhurst, T., Ellis, R., Koo, D. & Szalay, A., 1990, Nature, 343, 726
- Carlberg, R.G., Cowie, L.L., Songaila, A. & Hu, E.M., 1997, in press
- Clements, D.L. & Couch, W.J., 1996, MNRAS, in press
- Cohen, J.G., Hogg, D.W., Pahre, M.A. & Blandford, R., 1996, ApJ, 462, L9
- Colless, M. & Dunn, A.M., 1996, ApJ, 458, 435
- Cowie, L.L. et al, 1997, in preparation
- Cowie, L.L., Songaila, A., Hu, E.M. & Cohen, J.G., 1996, AJ, in press
- de Lapparent, V., Geller, M. & Huchra, J.P., 1986, ApJ, 302, L1
- de Vaucouleurs, G.H. 1975, in *Galaxies and the Universe*, ed. A.Sandage, M.Sandage, J. Kristian & G.Tammann, pg. 557
- Dressler, A. 1980, ApJ, 236, 351
- Hogg, D.W., Blandford, R.D., Kundić, T., Fassnacht, C.D. & Malhotra, S., 1996, ApJ, in press
- Kraan-Korteweg, R., 1981, AA, 104, 280
- Landy, S.D., Shectman, S.A., Lin, H., Kirshner, R.P., Oemler, A.A. & Tucker, D., 1996, ApJ, 456, L1
- LeFèvre, O., Hudon, D., Lilly, S.J., Crampton, D., Hammer, F. & Tresse, L., 1996, ApJ, 461, 534
- Oke, J.B., et al, 1995, PASP 107, 3750
- Park C.B. & Gott, J.R. 1991, MNRAS 249, 288
- Postman M.A., Lubin L.M., Gunn J.E., Oke J.B., Hoessel J.G., Schneider D.P., Christensen J.A., 1996, AJ, 111, 615

- Shandarin, S.F., Melott, A.L., Mcdavitt, K., Pauls, J.L. & Tinker, J., 1995, *PhysRevL*, 75, 7
- Steidel, C.C., Giavalisco, M., Dickinson, M. & Adelberger, K.L., 1996, *AJ*, in press
- Thompson, L.A. & Gregory, S.A., 1980, *ApJ*, 242, 1
- van den Bergh, S., Abraham, R.G., Ellis, R.S., Tanvir., N.R. & Santiago, B.X., 1996, preprint
- Williams, R.E., Blacker, B.S., Dickenson, M., Ferguson, H.C., Fruchter, A.S., Giavalisco, M., Gilliland, R.L., Lucas, R.A., McElroy, D.B., Petro, L.D. & Postman, M., 1996, in *Science with the Space Telescope - II*, ed. P.Benevenuti, F.D.Machetto & E.J.Schreier

Fig. 1.— The redshift histogram for the galaxies in the merged Caltech and Hawaii survey of the HDF.

Fig. 2.— The distribution of our sample of galaxies projected onto the sky is shown. Galaxies in the two most populous redshift peaks are indicated.



Hubble Deep Field - Caltech + Hawaii Data

